Journal of Applied Physics

RESEARCH ARTICLE | MAY 20 2021

Self-energized organic-inorganic hybrid composite for surface enhanced Raman spectroscopy

Diana T. Alvarez-Ruiz ; Sawsan Almohammed ; Agata Fularz ; Sebastian Tade Barwich; James H. Rice

J. Appl. Phys. 129, 193102 (2021)
https://doi.org/10.1063/5.0048802

Journal of Applied Physics ARTICLE scitation.org/journal/jap

Self-energized organic-inorganic hybrid composite for surface enhanced Raman spectroscopy

Cite as: J. Appl. Phys. **129**, 193102 (2021); doi: 10.1063/5.0048802
Submitted: 26 February 2021 · Accepted: 6 May 2021 ·
Published Online: 20 May 2021

Diana T. Alvarez-Ruiz,[1] Sawsan Almohammed,[1,2] Agata Fularz,[1] Sebastian Tade Barwich,[3] and James H. Rice[1,a)]

AFFILIATIONS

[1]School of Physics, University College Dublin, Belfield, Dublin 4 D04 V1W8, Ireland
[2]Conway Institute of Biomolecular and Biomedical Research, University College Dublin, Belfield, Dublin 4 D04 V1W8, Ireland
[3]School of Physics, Trinity College Dublin, Dublin 2 D02 PN40, Ireland

[a)]**Author to whom correspondence should be addressed:** james.rice@ucd.ie

ABSTRACT

In this study, we integrate plasmonic metal nanomaterials with a piezoelectric polyvinylidene fluoride (PVDF) polymer and lithium niobate ($LiNbO_3$) based composite to form an all-solid-state flexible self-energized sensor. We demonstrate that following the application of a load, the film enhances the surface-enhanced Raman spectroscopy (SERS) signal of an analyte molecule up to 14 times. The piezoelectric β-phase of PVDF in the film is optimized through the introduction of multi-walled carbon nanotubes and post-fabrication UV irradiation annealing. Additionally, the SERS signal enhancement can be further increased by the application of *in situ* UV light irradiation of the sample, resulting in the generation of photoexcited electrons from $LiNbO_3$ microparticles introduced into the composite. Both the application of a mechanical displacement and the UV light-induced charge generation result in an improved charge transfer between the film and an analyte molecule. The piezoelectric PVDF/$LiNbO_3$ film has been shown to be a suitable SERS platform for the detection of important biological molecules, demonstrating the potential of the substrate for fast on-site detection applications.

I. INTRODUCTION

The design and fabrication of chemical sensors with high sensitivity and selectivity have attracted considerable attention in fields such as environmental monitoring, medical diagnostics, and forensic analysis[1–16] Surface-Enhanced Raman Spectroscopy (SERS) is a powerful vibrational spectroscopic technique widely used in analytical chemistry that enables precise molecular identification.[17] The two key mechanisms contributing to the SERS enhancement are the electromagnetic[18] and chemical[19] mechanisms. The electromagnetic enhancement contribution results from the amplification of the local electromagnetic fields near nanostructured metals due to the excitation of localized surface plasmon resonances. The chemical enhancement mechanism arises from charge transfer between the SERS substrate and the analyte molecule. SERS enhancement may be ascribed to the electromagnetic and/or to the chemical mechanism, depending on the specific properties of the substrate and the analyte molecule. We aim to exploit both mechanisms simultaneously by using plasmon-active metallic nanostructures combined with a piezoelectric polyvinylidene fluoride (PVDF) polymer facilitating charge transfer, leading to better SERS efficiency of the substrate.

Electric-field up-regulated surface-enhanced Raman spectroscopy (E-SERS) has been shown to effectively increase Raman signal intensities through combining triboelectric or piezoelectric materials with plasmonic nanomaterials.[8,20,21] For instance, it has been demonstrated that the SERS signal from a probe molecule can be enhanced up to threefold by depositing it on a triboelectrically active material combined with Au–Ag nanostructures.[20] It has also been shown that a self-energizing substrate based on PVDF combined with graphene and silver nanowires provides electrical potential by converting film deformation from a finger press into stored electrical energy.[21] The E-SERS mechanism enables an increase in Raman signals up to ten times for a variety of analyte molecules.

Additionally, it has been shown that SERS signal intensities can be boosted through the application of light irradiation of a composite material containing both a metal and a semiconductor.

The photo-induced enhanced Raman spectroscopy (PIERS) mechanism has been demonstrated for gold nanoparticle/titanium dioxide (TiO_2) platforms.[22] The PIERS signal has been reported to be an order of magnitude higher than the SERS signal of a molecule prior to the super-bandgap pre-irradiation of the substrates. The additional enhancement in the Raman signal intensity has been assigned to more efficient charge transfer between the template and the analyte molecule.

Here, we report a strategy to increase the SERS signal levels by combining a SERS-active nanostructure with a flexible piezoelectric film based on a PVDF–silver nanoparticle (AgNPs) composite. This film used as a SERS substrate enables boosting of the Raman signal of analyte molecules by up to an order of magnitude through the application of a load to the piezoelectric film [Fig. 1(a)]. We propose that the SERS enhancement is observed following the conversion of the film deformation into stored electrical energy by the piezoelectric film. The charge generated by the application of mechanical stress can be transferred to an analyte molecule, resulting in a strengthened chemical enhancement mechanism. PVDF possesses high dielectric and piezoelectric constants[23] enabling a self-charging effect. In order to boost the piezoelectric properties of the film, multiwalled carbon nanotubes (MW-CNTs) have been interwoven into the PVDF composite, resulting in the increase of the concentration of the piezoelectric β-phase of PVDF. Ferroelectric lithium niobate ($LiNbO_3$) micro-sized particles were also added to the composite. Electronic transitions created through the application of super bandgap (UV) irradiation to $LiNbO_3$ can potentially create charges that transfer to the probe molecule. This process can boost the SERS signal of the probe molecule through a strengthened chemical enhancement mechanism. Moreover, other than supplying the required conditions for PIERS enhancement, UV treatment procedures have also been shown to increase the concentration of piezoelectric β-phase in PVDF. We propose that the combined effects of localized surface plasmon resonance excitation in the metal, stress-induced charge generation in PVDF, as well super-bandgap excitation in $LiNbO_3$ due to UV light irradiation result in a significant boost of the SERS signal. The approach is applied to a range of probe molecules including important biological molecules, demonstrating the potential of the substrate for fast on-site detection applications.

II. MATERIALS AND METHODS

A. Preparation of PVDF/$LiNbO_3$/MWC-NT composites

A schematic illustration of the fabrication process of the piezoelectric film-based SERS substrate is shown in Fig. 1(b). Nanocomposites based on polyvinylidene fluoride (PVDF) with different amounts of lithium niobate ($LiNbO_3$) and multi-wall carbon nanotubes (MW-CNTs) were prepared by the solvent casting method. The starting raw materials were reagent grade polyvinylidene fluoride (M_w: 534 000 determined by gel permeation

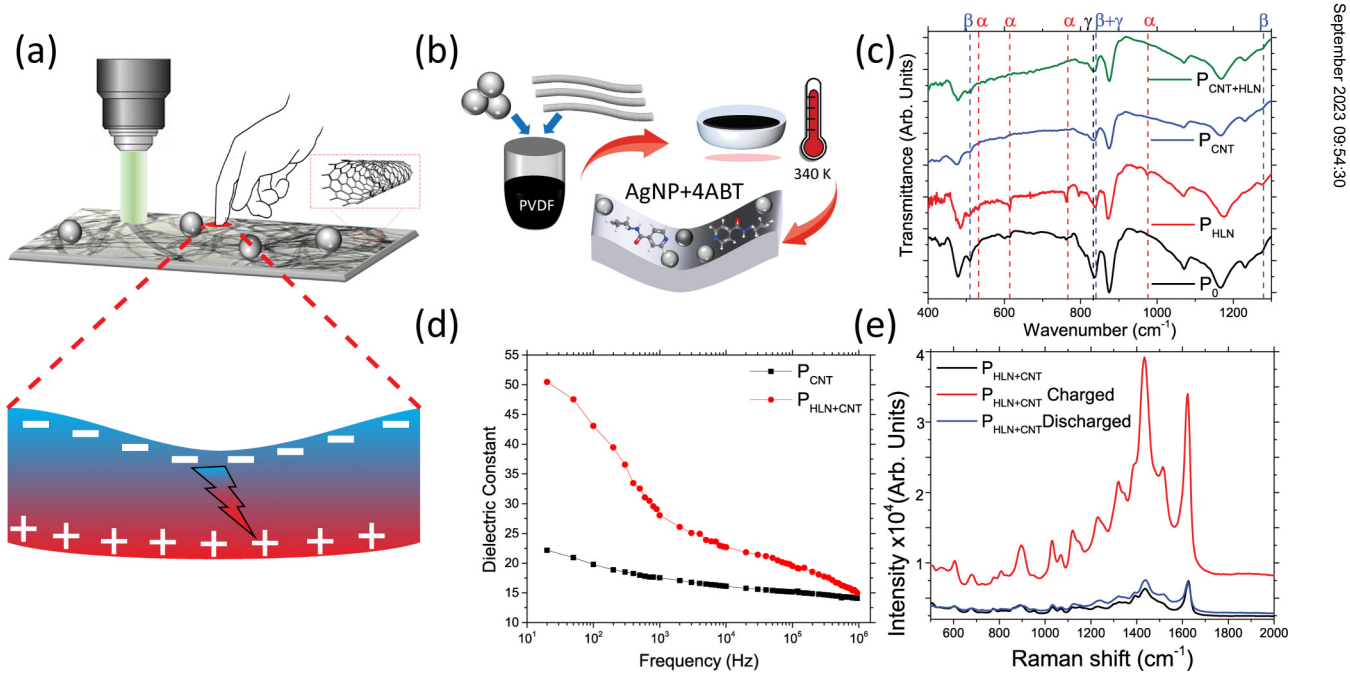

FIG. 1. (a) Schematic drawing of the $P_{HLN+CNT}$ composite film boosting the SERS signal by up to an order of magnitude through the application of a load due to the generation of a piezoelectric charge. (b) Schematic drawing of the synthesis process of the composite $P_{HLN+CNT}$ film. (c) FTIR spectra of four studied composite films. (d) The dielectric constant of P_{CNT} and $P_{HLN+CNT}$ samples. (e) SERS spectra of methylene blue added to $P_{HLN+CNT}$ before and after the application of weight of 420 g (applied at a 7 mm distance from the incident laser spot on the sample). Detailed sample composition is outlined in Table S1 in the supplementary material.

chromatography), lithium niobate (99.9%), and multi-wall carbon nanotubes (>90%, D × L 110–170 nm × 5–9 μm) obtained from Sigma Aldrich Ireland®. First, the suspension of 0.17 and 0.85M $LiNbO_3$ in dimethylformamide (DMF) (Honeywell®, 99.8%) was stirred with 0.25 wt./vol. % MW-CNTs for 1 h. The suspension was then sonicated for 1 h to breakup MW-CNTs agglomerates. 7.5 wt./vol. % PVDF was added to the $LiNbO_3$/MW-CNTs mixture and further stirred for 1 h at 340 K. 50 μl of the well-mixed suspension was drop cast on a coverslip heated to 340 K and left to dry for 1 h. For subsequent characterizations, the PVDF nanocomposite films were peeled off from the coverslips. For comparison purposes, composites without $LiNbO_3$ and MW-CNTs were prepared following the same methodology as described above. The details regarding sample composition are listed in Table S1 in the supplementary material. The thickness of the nanocomposite films reported here was about ∼300 μm and was kept constant regardless of the composition of the sample (MW-CNTs or $LiNbO_3$ loading).

B. Preparation of probe molecule solution

4-aminothiophenol (4-ABT, CAS 1193-02-8, New Star Chemical) powder was dissolved in methanol at an initial concentration of 10^{-2}M and then diluted in de-ionized water down to 10^{-4}M. Methylene blue (MB, CAS 122965-43-9, Sigma-Aldrich) and meso-tetra (*N*-methyl-4-pyridyl) porphine tetrachloride (TMPyP; T40125, Frontier Scientific) powders were dissolved in distilled water and then diluted down to a final concentration of 10^{-4}M. Thymine (T0376, Sigma-Aldrich) and cytosine (C3506, Sigma-Aldrich) were dissolved in de-ionized water at a concentration of 10^{-3}M, then stirred for around 30 min using a magnetic stirrer until the powder dissolved.

C. SERS measurements

For SERS measurements, 10 μl of silver nanoparticle suspension in water (CAS 795,968, Sigma-Aldrich) with a diameter of 40 nm and a concentration of 0.02 mg/ml was drop cast on the surface of the PVDF composite and then left to dry at room temperature. Subsequently, 10 μl of the probe molecule solution was drop cast on the top of the AgNPs and left to dry at room temperature until the solvent evaporated. The SERS spectra were measured using a bespoke Raman system, comprising an inverted optical microscope (IX71, Olympus®), a monochromatic green laser (532 nm, ThorLabs®) with a beam splitter and long pass filter (RazorEdge, Semrock®), a spectrograph (SP-2300i, Princeton Instruments®), and a CCD camera (IXON, Andor®). The 5 mW laser was focused using a 50× objective lens. For the loading experiment, a weight of 420 g was applied at a 7 mm distance from the incident laser spot on the sample. The effect of the applied load on the SERS spectra was studied immediately after the load was applied. The spectra were obtained in an accumulation mode (1 s integration time, accumulating 30 times) and the total acquisition time of the spectra was 30 s. The load was kept on the piezoelectric film while the data were being collected to ensure that the load was maintained during SERS acquisition. After 30 s, the load was removed and the data for the discharged film were measured. For UV light exposure SERS measurements, the composites with the plasmonic nanoparticles and analyte molecule on the surface were irradiated by a short-wave UV quartz pencil (Edmund Optics, #40-759, 253.7 nm, 4.89 eV, a nominal output power of 4.5 mW/cm^2) in 20-min increments up to a total irradiation time of 120 min. SERS measurements were taken when the UV lamp was off. Five measurements from one location on the same sample were taken and the average is reported; the spatial variability was assessed by averaging spectra recorded from three different locations.

D. Microscopy and spectroscopy characterization

Fourier transform infrared spectroscopy (FTIR) measurements were performed using an Alpha platinum-ATR spectrometer (12209186, Bruker®). The spectra were collected using transmission mode scanning from 400 to 4000 cm^{-1}, taking 64 scans per measurement with a resolution of 1 cm^{-1}.

Absorbance measurements were carried out using a UV–Vis spectrometer (V-650, JASCO, Inc.®) from 190 to 900 nm using a 1 nm step size, 1 nm bandwidth, and a scan speed of 400 nm/min.

Scanning electron microscopy (SEM) images of the composites were taken using a cold field emission (CFE) SEM operating at 5 kV (Regulus 8230, Hitachi-HighTech®). Prior to SEM imaging, a thin (∼8 nm) layer of iridium was sputtered (Quorum Q150T®) on the samples to avoid charging on the surface.

E. Dielectric measurements

Dielectric constant (ε) and ac conductivity (σ_{ac}) measurements were carried out using a parallel-plate capacitor structure. The capacitance (C) and tangent loss ($\tan\delta$) of the samples were measured using an HP 4284A® Precision LCR meter in the frequency range of 20 Hz to 1 MHz applying an electric field of 1 V. The dielectric constant was then evaluated using the parallel-plate capacitor equation: $\varepsilon = Cd/\varepsilon_0 A$, where d and A are the thickness and the area of the films, respectively. C is the capacitance of the sample and ε_0 is the permittivity of the free space (8.854×10^{-12} F/m). The ac conductivity was calculated using the following formula:

$$\sigma_{ac} = \omega \varepsilon_0 \varepsilon \tan\delta,$$

where ω is the angular frequency applied.

III. RESULTS AND DISCUSSION

Synthesized films were prepared through the mixing of PVDF, MW-CNTs, and $LiNbO_3$ in a solvent, followed by drop-casting and drying of the substrate [shown schematically in Fig. 1(b)]. The precise composition of the resulting samples is outlined in Table S1 in the supplementary material and Sec. II. PVDF composites containing $LiNbO_3$ and MW-CNTs (sample $P_{HLN+CNT}$) were first prepared. Infrared absorption spectroscopy (FTIR) showed that the $P_{HLN+CNT}$ sample contained electroactive β and γ phases [Fig. 1(c)]. SEM images of $P_{HLN+CNT}$ confirm that the composites consisted of homogenously distributed MW-CNTs and LN particles on a well-connected plain spherulites matrix of about 6 μm diameter [Figs. S2(b) and S2(c) in the supplementary material].

Such well-connected plain spherulites have been reported to be present when PVDF is formed in electroactive β and γ phases.[24]

The surface-enhanced Raman spectroscopy spectrum of methylene blue (MB) added to the $P_{HLN+CNT}$ sample as probe molecule was recorded and is shown in Fig. 1(e). The effect of pressing the substrate on the SERS spectra was then studied. The application of a load via pressing the sample surface [Fig. 1(e)] resulted in a tenfold increase in the SERS signal. The SERS signal intensity was reduced back to its original intensity following the removal of the load. The SERS spectra recorded show Raman bands consistent with the ones previously reported in the literature for methylene blue, i.e., peaks at 1623 cm^{-1} (ascribed to C—C ring stretching), 1436 cm^{-1} (C—N asymmetric stretching), and 1385 cm^{-1} (C—H in-plane ring deformation).[25]

The FTIR spectrum of PVDF without carbon nanotubes or lithium niobate added (sample P_0) [Fig. 1(c)] consisted of absorbance bands characteristic for α, β, and γ PVDF crystallites. Small absorbance bands of the α crystal are observed at 530 (CF_2 bending), 615 and 765 cm^{-1} (CF_2 bending and skeletal bending), and 976 cm^{-1} (CH out-of-plane deformation). Strong β and γ bands at 511 (β CF_2 bending), 833 (γ), 840 (β and γ), and 1279 cm^{-1} (β CF out-of-plane deformation) indicate that the sample consists of dominant ferroelectric β phase with a minor amount of electroactive γ and non-polar α phases. The addition of MW-CNTs to PVDF (sample P_{CNT}) [Fig. S2(a) in the supplementary material] suppressed the nucleation of the α polymorph. SEM images of P_{CNT} show a well-connected plain spherulites matrix of about 6 μm diameter [Figs. S2(b) and S2(c) in the supplementary material]. The data support the assertion that the addition of MW-CNTs results in the generation of electroactive β and γ PVDF phases.[24] FTIR spectroscopy showed that the incorporation of only $LiNbO_3$ into PVDF (P_{LN}) [Fig. 1(c)] did not prevent the nucleation of the α polymorph, however, the addition of MW-CNTs and $LiNbO_3$ together to PVDF did prevent the nucleation of the α polymorph within the sample showing predominant β and γ crystal phases.

PVDF films prepared with MW-CNTs and $LiNbO_3$ (sample $P_{HLN+CNT}$) were flexible and entirely black [Fig. 2(b)] suggesting that the MW-CNTs were homogeneously distributed in the composite at the macroscopic level in line with our SEM results. Based on the UV–Vis absorption data, the sample absorbs light in the UV region [Fig. 2(b)]. Current–voltage characteristic curves of the polymers with and without MW-CNTs were measured in the −5 to 5 V range to avoid excessive heating of the samples [Fig. 2(a)]. PVDF-based composites with small additions of MW-CNTs (with and without LN) showed a quasi-ohmic behavior, whereas samples without MW-CNTs were completely insulating and could not be measured using our experimental setup. The IV plot of P_{CNT} composites has been attributed to a tunneling effect in the electrical conductivity of the composite when the CNT concentration is close to the percolation threshold.[26] The conducting paths formed by the well-dispersed MW-CNTs help to reduce the internal resistance of the composite as well, which has been demonstrated to lead to short voltage lifetime and high output characteristics.[27]

The effect of $LiNbO_3$ addition on the dielectric properties, i.e., dielectric constant, tangent loss, and the ac conductivity of samples with MW-CNTs was studied in the 20 Hz–1 MHz frequency range and is shown in Figs. 1(d) and 3. The dielectric constant of the MW-CNT-containing samples is improved with $LiNbO_3$ addition, reaching the highest value of ∼50 at 0.85M incorporation of $LiNbO_3$ ($P_{HLN+CNT}$), while the dielectric constant of the sample containing only MW-CNT (P_{CNT}) was about 22 at the same frequency. The improvement in the dielectric constant through $LiNbO_3$ addition did not significantly diminish the dielectric losses at low frequencies. The relatively low dielectric loss observed in the MW-CNTs-containing samples (Fig. 3) further confirms the homogeneous distribution of the nanotubes throughout the sample. The mass percentage of conducting MW-CNTs in the composite was kept low (0.25 wt./vol. %) to facilitate the formation of the electroactive PVDF phases, decrease the internal resistance, and not affect the dielectric properties [Fig. 1(d)] of the composite.[26–31]

Based on the FTIR and SEM studies, we can see the role MW-CNTs play in preventing the nucleation of the paraelectric α phase and promotion of the β-phase. The electrical measurements further confirm that the role of MW-CNTs is not only limited to the formation of electroactive PVDF phases but also the decrease in the internal resistance of the PVDF films.

Further enhancement of the nucleation rate of electroactive β crystallite in the $P_{HLN+CNT}$ film was achieved by employing a simple and cost-effective method of exposing the film following drop-casting deposition to UV light irradiation ($\lambda_{ex} \sim 253.7$ nm). Exposure of $P_{HLN+CNT}$ to UV light promoted the γ to β phase transition, as can be observed in Fig. 2(c). The characteristic bands of the β polymorph (511 and 1279 cm^{-1}) become stronger at expense of the γ crystallite bands (833 and 1234 cm^{-1}). The left shoulder in the 840 cm^{-1} band commonly ascribed to γ (833 cm^{-1}) starts disappearing upon UV light exposure. Samples made with a low concentration of $LiNbO_3$ ($P_{LLN+CNT}$) produced a weaker conversion to the β-phase compared to when a higher concentration of $LiNbO_3$ is used ($P_{HLN+CNT}$).

The γ to β or α to β phase transformation upon UV light exposure was not observed in samples prepared with pure PVDF (sample P_0) or samples prepared by adding only MW-CNTs to PVDF (sample P_{CNT}) composites [Fig. S2(b) in the supplementary material]. Due to the attention directed to the β phase and its superior ferroelectric performance, the γ phase has been previously mistakenly reported in the literature as the β phase.[32] Here, we unambiguously show the γ to β phase transition by accurately assigning the γ and β bands in our FTIR spectra.

The UV light irradiation of the substrate may be used not only to increase the concentration of the piezoelectric β-phase in the film but also to boost the charge generation in $LiNbO_3$ via the previously described PIERS mechanism. Measuring the SERS signal intensity from a probe molecule recorded on $P_{HLN+CNT}$ as a function of UV irradiation time showed that the Raman signal intensity increased with UV irradiation time. A greater than tenfold increase in SERS intensity from 4-ABT adsorbed onto AgNPs was achieved using $P_{HLN+CNT}$ after 100 min of UV light exposure [Fig. 2(d)]. The SERS spectra of 4-ABT possess features in agreement with those reported in the literature, e.g., four b_2 (at 1142, 1390, 1433, and 1575 cm^{-1}) and one a_1 (1082 cm^{-1}, C-S stretching) symmetry species of benzene ring vibrations.[33] To show the reproducibility, ten continuous measurements of charging/discharging cycles were recorded using the $P_{HLN+CNT}$ composite, shown in [Fig. 2(e)].

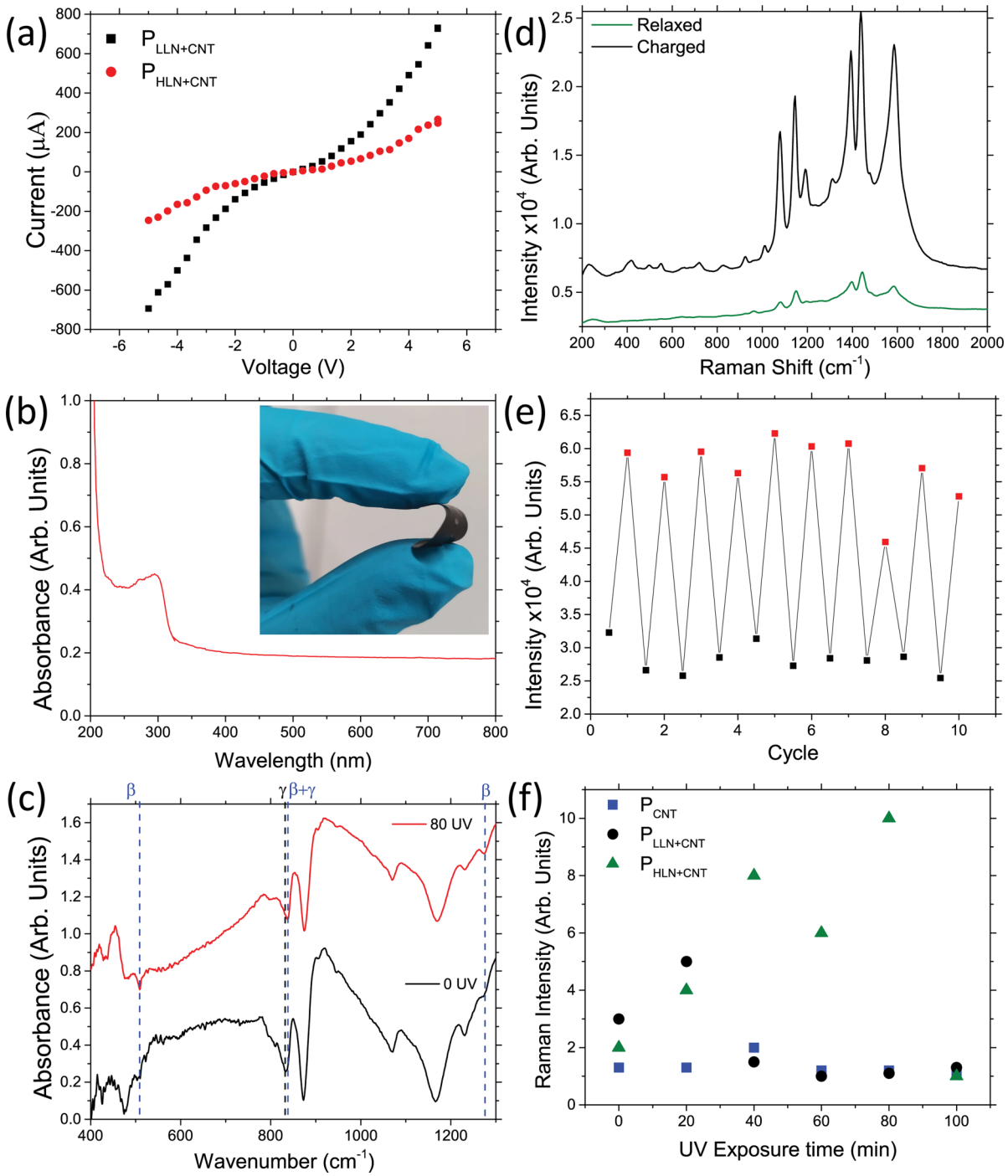

FIG. 2. (a) Current–voltage characteristic (I–V plot) curve of $P_{LLN+CNT}$ and $P_{HLN+CNT}$ samples. (b) UV–Vis absorption spectra of the $P_{HLN+CNT}$ composite. The inset shows a picture of the substrate demonstrating its flexibility. (c) FTIR spectra of $P_{HLN+CNT}$ before and following 30 min of UV exposure. (d) SERS spectra of probe molecule 4-ABT on $P_{HLN+CNT}$ under periodic load application (charged) and following removal of the load (relaxed). (e) SERS intensity of the highest intensity peak in the 4-ABT spectrum on $P_{HLN+CNT}$ under periodic load application and relaxation cycles. (f) SERS signal intensity following mechanical deformation due to the application of a weight of 420 g (applied at a 7 mm distance from the incident laser spot on the sample) as a function of UV exposure time. Detailed sample composition is outlined in Table S1 in the supplementary material.

Small variations in the Raman intensity are observed due to the variations in the force exerted in each cycle.

The SERS of 4-ABT spectra prior to UV light exposure (i.e., 0 min exposure time) was studied for three composites (e.g., P_{CNT}, P_{LLN}, and P_{HLN}) following mechanically deforming the sample through the application of a load [Fig. 2(f)]. The SERS spectra showed a 1.6-fold enhancement in signal intensity for P_{CNT}, while P_{LLN} and P_{HLN} composites showed a 2.7- and 2.3-fold enhancement, respectively [Fig. 2(f)]. Following these studies, we then assessed the impact of UV exposure on the SERS signal intensity of 4-ABT from all three composites. Composites containing $LiNbO_3$ particles exhibited a superior SERS performance compared to PVDF samples containing only MW-CNTs. Examination of the plot [Fig. 2(f)] shows that a sufficient amount of $LiNbO_3$ is required to optimize the impact of UV irradiation of the substrate in order to maximize the enhancement in SERS signal levels. Noting that due to the diminishing effect of the paraelectric α phase on the piezoelectric performance of the P_0 and P_{HLN} samples, samples without MW-CNTs were not further studied for SERS applications. We propose that the role of $LiNbO_3$ in enhancing the SERS signal intensities is through the application of super-bandgap UV irradiation through PIERS.[22] The effect of *in situ* UV light irradiation on lithium niobate on insulator (LNOI)–silver nanoparticle templates was previously described in detail in the literature.[34] $LiNbO_3$ is a wide-bandgap semiconductor (bandgap of ~3.9 eV), and it can be directly excited by UV light of energy equal to 4.8 eV (253.7 nm). We believe that the main mechanism following UV irradiation charge generation in the $LiNBO_3$ particles in the PVDF film, which are later transferred to the probe molecule, resulting in an enhancement of the SERS signal via the chemical enhancement mechanism. UV light exposure can potentially generate shallow defects in the $LiNbO_3$ crystal.[10,22] Electronic transitions from the defect-related energy levels can be driven by the laser used for the Raman measurements; the charges excited can then transfer to the probe molecule from the substrate. This electron transfer process can enhance the Raman signal intensity of the probe molecules through a chemical enhancement mechanism. Such a process has been proposed to explain PIERS in previous studies.[10,22]

The SERS signal of an analyte molecule deposited on the P_{CNT} sample that did not contain $LiNbO_3$ remained constant throughout the measurement for up to 100 min of UV exposure. Therefore, we believe that the molecule used in the experiment is stable under UV irradiation for the duration of time used in the experiment, and any changes observed in the intensity of the spectrum are due to additional charge generation after super-bandgap excitation in $LiNbO_3$.[35] Longer UV irradiation exposure times affected the SERS signal of the analyte molecule due to possible photooxidative effects.[36]

In order to demonstrate the universality of the method and the potential of the piezoelectric $P_{HLN+CNT}$ substrate for biomolecule monitoring applications, the load application method was employed for three additional analyte molecules, as shown in Fig. 4. Porphyrins such as TMPyP are conjugated organic molecules that can self-assemble into nanoscale superstructures that appear in many biological systems.[37] Due to the high light-harvesting efficiencies of such systems, porphyrins have potential applications in solar energy harvesting and organic electronics.[38] The Raman spectrum of TMPyP on the $P_{HLN+CNT}$ substrate is characterized by peaks at 1249 cm^{-1} (C-pyrrole bending), 1451 and 1557 cm^{-1} (C–C stretching), as well as 1639 cm^{-1} (pyrrole bending) in agreement with values previously reported in the literature.[10,39] Following the application of the load, the relative intensity of the peaks increased twofold. Additionally, two nucleobases, thymine and cytosine, were investigated as analyte molecules. Detection of DNA or RNA sequences is of high importance in the field of diagnostics and early disease detection;[40] nucleobases are, however, difficult to detect using SERS due to their low Raman

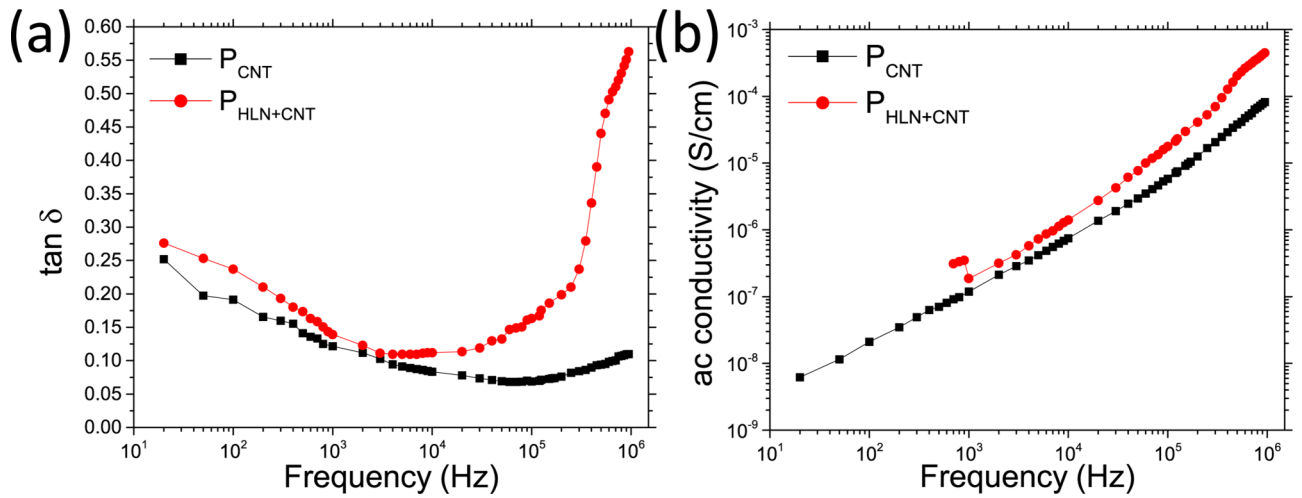

FIG. 3. (a) Dielectric losses and (b) ac conductivity of $P_{HLN+CNT}$ and P_{CNT} samples.

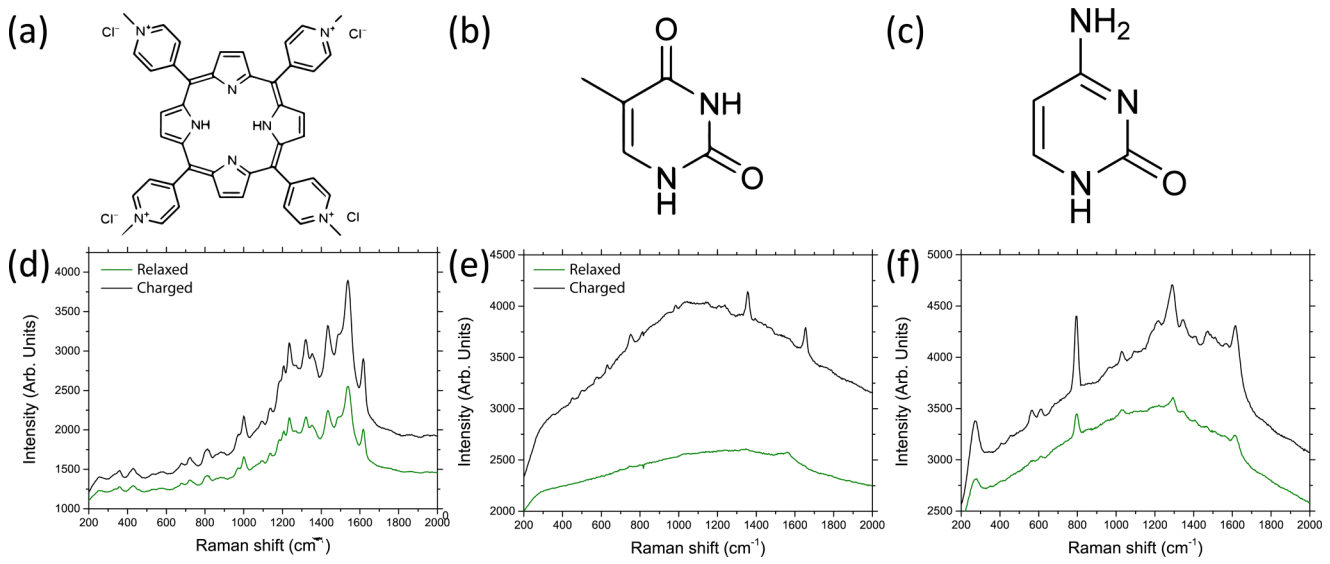

FIG. 4. Structure of the molecule (a)–(c) and SERS spectra (d)–(f) of (a) and (d) TMPyP, (b) and (e) thymine, and (c) and (f) cytosine added to $P_{HLN+CNT}$ before and after the application of a weight of 420 g (applied at a 7 mm distance from the incident laser spot on the sample).

cross sections.[41] When thymine is deposited on the polymer substrate only one peak at 1655 cm^{-1}, which was previously reported to be the marker band of thymine associated with C═O stretching, can be seen.[40,42] Following the application of the load the peak intensity is enhanced fourfold and additional peaks at 574 cm^{-1} (ring deformation) 752 cm^{-1} (ring breathing), and 1356 cm^{-1} (CH_3 bending and C—H deformation)[42] appear in the spectrum. The spectrum of cytosine is characterized by peaks at 562 cm^{-1} (ring deformation), 797 cm^{-1} (ring breathing), 1289 cm^{-1} (ring stretching C—N), and 1617 cm^{-1} (C═O stretching) among others in agreement with values reported in the literature.[42] The intensity of the cytosine peaks was enhanced up to fourfold following the application of the load.

IV. CONCLUSIONS

We have reported nucleation of single β-phase PVDF film by the use of $LiNbO_3$/MW-CNTs sample loading and post-treatment UV light irradiation. The fabricated piezoelectric PVDF composites could be applied as self-energized touch sensors able to enhance the SERS response of different analyte molecules including important biomolecules. A higher than tenfold increase was observed after the application of a load to the piezoelectric film with a high $LiNbO_3$ concentration (0.85M). Compared with samples containing the paraelectric α phase, single β phase PVDF composites significantly increased the SERS enhancement of analyte molecules in response to the applied mechanical stress. Samples with higher $LiNbO_3$ loading showed enhanced SERS response when being pressed after UV radiation exposure. The enhanced SERS signal is attributed to a combination of two charge transfer mechanisms: the first one produced as a consequence of the mechanical stress applied to the piezoelectric PVDF film; the second one resulting from the promotion of UV-photoexcited electrons from the $LiNbO_3$ particles to the analyte molecule, resulting in the number of Raman photons emitted.

SUPPLEMENTARY MATERIAL

See the supplementary material for SEM and FTIR data as well as the composition of the samples.

ACKNOWLEDGMENTS

The authors thank Ian Reid for access to SEM, Gareth Redmond for access to UV−Vis, and Aaron Martin for access to FTIR. This publication has emanated from research conducted with the financial support of the UCD School of Physics (SIRAT—Scholarship in Research and Teaching). The work was supported by Science Foundation Ireland (No. 18/TIDA/6139) and Sustainable Energy Authority of Ireland (SEAI) (No. 18/RRD/0033).

DATA AVAILABILITY

The data that support the findings of this study are available from the corresponding author upon reasonable request.

REFERENCES

[1]L. Guerrini, N. Pazos-Perez, E. Garcia-Rico, and R. Alvarez-Puebla, Cancer Nanotechnol. **8**, 5 (2017).
[2]S. Chen, L. Dong, M. Yan, Z. Dai, C. Sun, and X. Li, R. Soc. Open Sci. **5**, 171488 (2018).
[3]S. S. Sinha, S. Jones, A. Pramanik, and P. C. Ray, Acc. Chem. Res. **49**, 2725 (2016).

[4]S. Damm, F. Lordan, A. Murphy, M. McMillen, R. Pollard, and J. H. Rice, Plasmonics **9**, 1371 (2014).
[5]T. J. Moore, A. S. Moody, T. D. Payne, G. M. Sarabia, A. R. Daniel, and B. Sharma, Biosensors **8**, 46 (2018).
[6]E. Kennedy, R. Al-Majmaie, M. Al-Rubeai, D. Zerulla, and J. H. Rice, RSC Adv. **3**, 13789 (2013).
[7]S. Almohammed, S. Tade Barwich, A. K. Mitchell, B. J. Rodriguez, and J. H. Rice, Nat. Commun. **10**, 2496 (2019).
[8]S. Almohammed, F. Zhang, B. J. Rodriguez, and J. H. Rice, J. Phys. Chem. Lett. **10**, 1878 (2019).
[9]R. M. Al-Shammari, N. Al-Attar, M. Manzo, K. Gallo, B. J. Rodriguez, and J. H. Rice, ACS Omega **3**, 3165 (2018).
[10]S. Almohammed, F. Zhang, B. J. Rodriguez, and J. H. Rice, Sci. Rep. **8**, 3880 (2018).
[11]S. Damm, S. Fedele, A. Murphy, K. Holsgrove, M. Arredondo, R. Pollard, J. N. Barry, D. P. Dowling, and J. H. Rice, Appl. Phys. Lett. **106**, 183109 (2015).
[12]N. Al-Attar, I. Kopf, E. Kennedy, K. Flavin, S. Giordani, and J. H. Rice, Chem. Phys. Lett. **535**, 146 (2012).
[13]S. Almohammed, S. O. Oladapo, K. Ryan, A. L. Kholkin, J. H. Rice, and B. J. Rodriguez, RSC Adv. **6**, 41809 (2016).
[14]J. H. Na, R. A. Taylor, J. H. Rice, J. W. Robinson, K. H. Lee, Y. S. Park, C. M. Park, and T. W. Kang, Appl. Phys. Lett. **86**, 113108 (2005).
[15]J. H. Rice, R. Aures, J. P. Galaup, and S. Leach, Chem. Phys. **263**, 401 (2001).
[16]S. Fedele, M. Hakami, A. Murphy, R. Pollard, and J. Rice, Appl. Phys. Lett. **108**, 053102 (2016).
[17]M. Fleischmann, P. J. Hendra, and A. J. McQuillan, Chem. Phys. Lett. **26**, 163 (1974).
[18]D. L. Jeanmaire and R. P. Van Duyne, J. Electroanal. Chem. **84**, 1 (1977).
[19]M. G. Albrecht and J. A. Creighton, J. Am. Chem. Soc. **99**, 5215 (1977).
[20]H. Li, H. Dai, Y. Zhang, Y. H. Lee, C. S. L. Koh, G. C. Phan-Quang, W. Tong, Y. Zhang, H. Gao, X. Y. Ling, and Q. An, Nano Energy **64**, 103959 (2019).
[21]H. Li, H. Dai, Y. Zhang, W. Tong, H. Gao, and Q. An, Angew. Chem. Int. Ed. **56**, 2649 (2017).
[22]S. Ben-Jaber, W. J. Peveler, R. Quesada-Cabrera, E. Cortés, C. Sotelo-Vazquez, N. Abdul-Karim, S. A. Maier, and I. P. Parkin, Nat. Commun. **7**, 12189 (2016).
[23]H. Kawai, Jpn. J. Appl. Phys. **8**, 975 (1969).
[24]E. Thangavel, S. Ramasundaram, S. Pitchaimuthu, S. W. Hong, S. Y. Lee, S. S. Yoo, D. E. Kim, E. Ito, and Y. S. Kang, Compos. Sci. Technol. **90**, 187 (2014).
[25]G. N. Xiao and S. Q. Man, Chem. Phys. Lett. **447**, 305 (2007).
[26]A. Ferreira, M. T. Martínez, A. Ansón-Casaos, L. E. Gómez-Pineda, F. Vaz, and S. Lanceros-Mendez, Carbon **61**, 568 (2013).
[27]K. I. Park, M. Lee, Y. Liu, S. Moon, G. T. Hwang, G. Zhu, J. E. Kim, S. O. Kim, D. K. Kim, Z. L. Wang, and K. J. Lee, Adv. Mater. **24**, 2999 (2012).
[28]E. Kabir, M. Khatun, L. Nasrin, M. J. Raihan, and M. Rahman, J. Phys. D: Appl. Phys. **50**, 163002 (2017).
[29]M. Castellino, M. Rovere, M. I. Shahzad, and A. Tagliaferro, Compos., Part A **87**, 237 (2016).
[30]J. Nunes-Pereira, P. Sharma, L. C. Fernandes, J. Oliveira, J. A. Moreira, R. K. Sharma, and S. Lanceros-Mendez, Compos., Part B **142**, 1 (2018).
[31]Y. W. Nam, W. N. Kim, Y. H. Cho, D. W. Chae, G. H. Kim, S. P. Hong, S. S. Hwang, and S. M. Hong, Macromol. Symp. **249–250**, 478 (2007).
[32]P. Martins, A. C. Lopes, and S. Lanceros-Mendez, Prog. Polym. Sci. **39**, 683 (2014).
[33]M. Osawa, N. Matsuda, K. Yoshii, and I. Uchida, J. Phys. Chem. **98**, 12702 (1994).
[34]R. M. Al-Shammari, M. A. Baghban, N. Al-attar, A. A. Gowen, K. Gallo, J. H. Rice, and B. J. Rodriguez, ACS Appl. Mater. Interfaces **10**, 30871 (2018).
[35]R. M. Al-Shammari, M. A. Baghban, N. Al-attar, A. Gowen, K. Gallo, J. H. Rice, and B. J. Rodriguez, ACS Appl. Mater. Interfaces **10**, 30871 (2018).
[36]Y. H. Chiu, T. F. M. Chang, C. Y. Chen, M. Sone, and Y. J. Hsu, Catalysts **9**, 430 (2019).
[37]Z. Wang, C. J. Medforth, and J. A. Shelnutt, J. Am. Chem. Soc. **126**, 15954 (2004).
[38]J. Ducke, A. Riss, A. Pérez Paz, K. Seufert, M. Schwarz, M. Garnica, A. Rubio, and W. Auwärter, ACS Nano **12**, 2677 (2018).
[39]B. Vlčková, P. Šmejkal, M. Michl, M. Procházka, P. Mojzeš, F. Lednický, and J. Pfleger, J. Inorg. Biochem. **79**, 295 (2000).
[40]R. A. Karaballi, A. Nel, S. Krishnan, J. Blackburn, and C. L. Brosseau, Phys. Chem. Chem. Phys. **17**, 21356 (2015).
[41]S. Almohammed, B. J. Rodriguez, and J. H. Rice, Sens. Biosens. Res. **24**, 100287 (2019).
[42]F. Madzharova, Z. Heiner, M. Gühlke, and J. Kneipp, J. Phys. Chem. C **120**, 15415 (2016).